

2019

Progressive Hypoxia-on-a-chip: An In Vitro Oxygen Gradient Model for Capturing the Effects of Hypoxia on Primary Hepatocytes in Health and Disease

Young Bok Abraham Kang
George Fox University, ykang@georgefox.edu


Jinsu Eo
Harvard Medical School

Beyza Bulutoglu
Harvard Medical School

Martin L. Yarmush
Rutgers University

O. Berk Usta
Harvard Medical School

Follow this and additional works at: https://digitalcommons.georgefox.edu/mece_fac

 Part of the [Biomedical Engineering and Bioengineering Commons](#), [Hepatology Commons](#), and the [Medical Sciences Commons](#)

Recommended Citation

Kang, Young Bok Abraham; Eo, Jinsu; Bulutoglu, Beyza; Yarmush, Martin L.; and Usta, O. Berk, "Progressive Hypoxia-on-a-chip: An In Vitro Oxygen Gradient Model for Capturing the Effects of Hypoxia on Primary Hepatocytes in Health and Disease" (2019). *Faculty Publications - Biomedical, Mechanical, and Civil Engineering*. 89.
https://digitalcommons.georgefox.edu/mece_fac/89

This Article is brought to you for free and open access by the Department of Biomedical, Mechanical, and Civil Engineering at Digital Commons @ George Fox University. It has been accepted for inclusion in Faculty Publications - Biomedical, Mechanical, and Civil Engineering by an authorized administrator of Digital Commons @ George Fox University. For more information, please contact arolfe@georgefox.edu.

Progressive hypoxia-on-a-chip: An in vitro oxygen gradient model for capturing the effects of hypoxia on primary hepatocytes in health and disease

Young Bok (Abraham) Kang^{1,2} | Jinsu Eo¹ | Beyza Bulutoglu¹ | Martin L. Yarmush^{1,3} |
O. Berk Usta¹

¹Department of Surgery, Center for Engineering in Medicine, Harvard Medical School, Massachusetts General Hospital, Shriners Hospitals for Children-Boston, Boston, Massachusetts

²Department of Mechanical & Civil & Biomedical Engineering, College of Engineering, George Fox University, Newberg, Oregon

³Department of Biomedical Engineering, Rutgers University, Piscataway, New Jersey

Correspondence

O. Berk Usta, Department of Surgery, Center for Engineering in Medicine, Harvard Medical School, Massachusetts General Hospital, Shriners Hospitals for Children-Boston, 51 Blossom Street, Boston, MA 02114.
Email: berkusta@gmail.com
and ousta@mgh.harvard.edu

Funding information

National Institutes of Health, Grant/Award Numbers: 1F32EB026916, 1R21EB020192, 5P41EB002503, 5R01EB023812; Shriners Hospital for Children, Grant/Award Number: 84311

Abstract

Oxygen is vital to the function of all tissues including the liver and lack of oxygen, that is, hypoxia can result in both acute and chronic injuries to the liver in vivo and ex vivo. Furthermore, a permanent oxygen gradient is naturally present along the liver sinusoid, which plays a role in the metabolic zonation and the pathophysiology of liver diseases. Accordingly, here, we introduce an in vitro microfluidic platform capable of actively creating a series of oxygen concentrations on a single continuous microtissue, ranging from normoxia to severe hypoxia. This range approximately captures both the physiologically relevant oxygen gradient generated from the portal vein to the central vein in the liver, and the severe hypoxia occurring in ischemia and liver diseases. Primary rat hepatocytes cultured in this microfluidic platform were exposed to an oxygen gradient of 0.3–6.9%. The establishment of an ascending hypoxia gradient in hepatocytes was confirmed in response to the decreasing oxygen supply. The hepatocyte viability in this platform decreased to approximately 80% along the hypoxia gradient. Simultaneously, a progressive increase in accumulation of reactive oxygen species and expression of hypoxia-inducible factor 1 α was observed with increasing hypoxia. These results demonstrate the induction of distinct metabolic and genetic responses in hepatocytes upon exposure to an oxygen (/hypoxia) gradient. This progressive hypoxia-on-a-chip platform can be used to study the role of oxygen and hypoxia-associated molecules in modeling healthy and injured liver tissues. Its use can be further expanded to the study of other hypoxic tissues such as tumors as well as the investigation of drug toxicity and efficacy under oxygen-limited conditions.

KEYWORDS

hepatocytes, HIF, hypoxia, microfluidics, oxygen gradient, ROS

1 | INTRODUCTION

Oxygen and its availability are vital to the function of tissues and cellular processes in both health and disease. Variations in oxygen levels through regular physiological processes and/or changes of oxygen supply into blood and tissues due to disease, sudden trauma,

or other injuries, are important determinants of cell metabolism and survival. The availability of oxygen can also be highly modulated for thick cancerous tissues, that is, tumors, and for external/internal wounds both of which result in poor oxygenation of a significant amount of cells in the specific tissue. Such deprivation of oxygen supply is called “hypoxia”. In the case of wounds, it has been well

documented that such hypoxia leads to significantly slower healing responses (Castilla, Liu, & Velazquez, 2012). In contrast, the highly hypoxic environment—especially at the core—of a tumor leads cellular adaptations for cancer cells which promote their survival through activation of glycolysis pathway genes among others (Covello et al., 2006; Keith, Johnson, & Simon, 2011; Moreno-Manzano et al., 2010).

The liver, with its significantly high oxygen consumption under normal conditions, is particularly of interest in terms of its responses to natural and gradual gradients of oxygen concentration in the liver sinusoid, and also to hypoxia during a traumatic event or disease. In a healthy liver tissue—along with other genetic, hormonal, and nutritional drivers—a gradient of oxygen due to its consumption along the sinusoid is an important driver of metabolic heterogeneity of the liver tissue which is specifically termed as “liver zonation”. In healthy liver tissue, the periportal blood with an oxygen partial pressure of 60–65 mmHg (7.9–8.6% O₂) flows into the liver sinusoid and drains out to the central vein at an oxygen partial pressure of 30–35 mmHg (3.9–4.6% O₂; Brooks, Eastwood, Beckingham, & Girling, 2004; Brooks, Hammond, Girling, & Beckingham, 2007; Kietzmann, 2017; M, 1996; Wolffe, Schmidt, & Jungermann, 1983).

Perhaps more importantly, this physiological oxygen gradient is also a driver of both heterogeneity and progressive development of disease (Bulutoglu et al., 2019; Hall et al., 2017), as demonstrated in our recent work that recapitulated the oxygen mediated zonation of lipid accumulation (Bulutoglu et al., 2019). A diseased and/or traumatically injured liver tissue further exhibits abnormal symptoms such as loss of normal hepatic metabolic functions, disrupted homeostasis, and inflammation (Albillos, Lario, & Alvarez-Mon, 2014; Nath & Szabo, 2012; Robinson, Harmon, & O’Farrelly, 2016). These symptoms are often closely associated with insufficient oxygen supply and severe hypoxia corresponding to <2% O₂. Prolonged oxygen tension below this 2% threshold level disrupts the oxygen balance and is characterized as tissue ischemia. This results in abnormal hepatic metabolic function due to the activation and release of key mediators such as reactive oxygen species (ROS) and hypoxia-inducible factors (HIFs). ROS are commonly upregulated during pathogenesis and pathological state; and subsequently accelerate liver injury and disease including liver fibrosis, steatosis, and liver cancer (Figure 1; Carreau, El Hafny-Rahbi, Matejuk, Grillon, & Kieda, 2011; Nath & Szabo, 2012; Paik, Jung, Lee, Park, & Lee, 2017; Semenza, 2012). In general, such disruption of oxygen supply plays a crucial role in the process of liver pathophysiology and pathogenesis (Ebert, 2006; Jaeschke, 2000; Lefere et al., 2016; Nath & Szabo, 2012).

Despite this vital importance of oxygen availability, the cellular mechanisms and regulatory machinery associated with hypoxia, ROS, and HIFs in the healthy and diseased liver tissues are not well investigated. While few studies attempt to study the effect of oxygen concentration on liver physiology, they are limited by their physiologically irrelevant oxygen concentrations. Most of these platforms involve 2D well plate cultures, which can simulate one zone of the liver at a time, use a reference point of 20% O₂ (the

atmospheric oxygen pressure), and focus on 1% or 2% O₂ to mimic hypoxia (Carreau et al., 2011; Copple, 2010; Popovici et al., 2001; Qin et al., 2015). These conditions do not reflect the *in vivo* liver microenvironment with continuous tissue under an oxygen gradient presence (Figure 1). Some of the more advanced platforms, simulating a physiologically relevant zonation, still have limitations as they employ passive oxygen gradient generation, where the gradients are generated by cellular consumption (Allen, Khetani, & Bhatia, 2005; Camp & Capitano, 2007; Cho et al., 2007; Park, Berthiaume, Toner, Yarmush, & Tilles, 2005). Similarly, spheroid models can naturally give rise to the spontaneous creation of oxygen gradients (Anada, Fukuda, Sai, & Suzuki, 2012; Ko et al., 2019; Yu et al., 2017); however, the reproducibility of such gradients relies heavily on both the tight distribution of spheroid sizes and the highly reproducible oxygen consumption rates of cells.

A recent study demonstrated an actively-controlled oxygen gradient model, generated in an open-well cell culture, where oxygen diffusion occurred through gas-permeable polydimethylsiloxane (PDMS; Lo, Sinkala, & Eddington, 2010). One limitation of this microfluidic platform is the discrepancy of oxygen levels along with the media at the top and the bottom of the cell culture. Another study recapitulated an oxygen gradient of 4–9% achieved by oxygen diffusion from air-gas (20% O₂ and 5% CO₂). A statistically significant change in expression levels of PEPCCK and GK enzymes, upregulated in periportal and pericentral regions, respectively, was demonstrated in two zones of the device (Sato, Kadokura, Uchida, & Tsukada, 2014). Several other microfluidic devices have been presented to create controllable hypoxia (oxygen) gradients using mixtures of oxygen-nitrogen gases (Allen et al., 2005; Camp & Capitano, 2007; Chang et al., 2014; De Miguel et al., 2016; Lo et al., 2010; Polinkovsky, Gutierrez, Levchenko, & Groisman, 2009). Based on our experience, the use of gas diffusion via a membrane may alter CO₂ concentration and cause air bubble generation within the device. Moreover, these devices showed some limitations in providing distinct sample collection to analyze the functional and metabolic activities of cells differentially expressed along an oxygen gradient.

A multizone oxygen gradient model, allowing for sample collection from different gradient sections, would be a step forward, that can simultaneously capture both normoxic and hypoxic conditions in a single microfluidic device on a single connected tissue. This approach can facilitate more gradual and comprehensive demonstration of zone-specific metabolic activity and gene expression profile of hepatocytes exposed to oxygen gradients. In addition, such technology would allow for the investigation of the effects of hypoxia on hepatocytes under healthy conditions and in the pathophysiological state of liver tissue. In our previous studies, we developed a microfluidic platform, the “Metabolic Patterning on a Chip (MPOC) device”, and successfully demonstrated *in vitro* zonation of primary rat and human hepatocytes via this platform. The MPOC device was able to create actively-controlled gradients of inducers or hormones, and thus enforce the creation of metabolic patterns across microscopic tissues (Kang, Eo, Mert, Yarmush, & Usta, 2018; McCarty, Usta, & Yarmush, 2016).

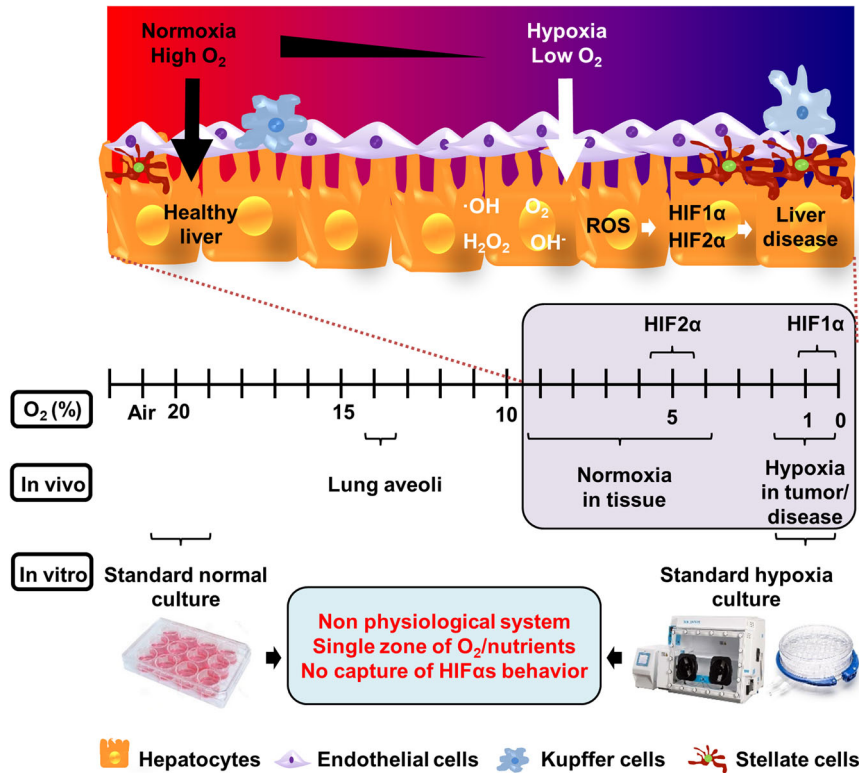


FIGURE 1 Oxygen levels in the liver under normoxic and hypoxic conditions. The oxygen ranges of the normoxia-hypoxia for both the human liver and the rat liver are similar. Under normoxia, the liver operates in an oxygen range of 3.9–8.6%. In liver ischemia and injured liver tissue, hypoxia corresponding to <2% O₂ is observed. Hypoxia causes reactive oxygen species (ROS) accumulation in cells, which leads to cellular damage and eventually to apoptosis. Hypoxia-associated factors (e.g., HIFs) are expressed under hypoxic conditions to protect cells from oxidative stress and to adjust to the oxygen-deprived environment. Non-parenchymal cells (e.g., hepatic stellate cells and Kupffer cells) are also activated under hypoxia. Cell culture systems using a standard well plate and a hypoxic chamber are not physiologically relevant systems as they capture a single zone of oxygen and nutrients. These cannot fully capture the different behaviors of HIFs that are activated at different oxygen levels in vivo [Color figure can be viewed at wileyonlinelibrary.com]

Here, we used the MPOC device to introduce an in vitro oxygen/hypoxia gradient for a short-time period in the range of 0.3–6.9% O₂ using a chemical oxygen-quenching approach (Jiang et al., 2011). At the maximum level, this oxygen concentration range represents an average oxygen tension value for healthy liver tissue and at the lowest end, it represents a severely hypoxic condition. Through this approach, we were able to understand and contrast hepatic phenotypes under normal oxygenation levels and severe hypoxia, which represents conditions such as acute injuries, temporary disruptions to the blood supply, and ischemia. Specifically, we assessed the short-term responses to an oxygen gradient in a liver microtissue of primary rat hepatocytes in terms of hypoxia-associated factors (e.g., ROS and HIFs) and confirmed the formation of a patterned molecular injury response across the MPOC device. Since here we only focused on short-term and primarily traumatic/ischemic injury phenotypes, we did not assess the zoned phenotypes and metabolism of hepatocytes which usually take about 24–48 hr to establish (Berndt & Holzhtuter, 2018; Cassim, Raymond, Lapiere, & Bilodeau, 2017). However, long-term studies are indeed possible with oxygen concentrations in full physiological range in the

MPOC device toward recapitulation of the effects of oxygen tension on the progression of certain diseases such as nonalcoholic fatty liver disease (NAFLD) (Bulutoglu et al., 2019).

2 | MATERIALS AND METHODS

2.1 | Microfluidic device design and fabrication

The design and fabrication of the gradient-generating MPOC device were explained in detail in our previous study (Kang et al., 2018). Briefly, it is composed of a gradient generator (width [w] × height [h]: 75 × 200 μm) and a cell culture chamber (wiggle shape, w × h × length [l]: 10,000 × 200 × 1,700 μm), in addition to inlets and outlets for media flow and cell seeding. All devices used in this study were fabricated by PDMS replica molding from a SU-8 template made with the help of photolithography technology, as previously described (Kang et al., 2018; McCarty et al., 2016). The PDMS microfluidic device was bonded on a glass microscope slide (w × l: 25 × 75 mm; Thermo Fisher Scientific, Grand Island, NY) after oxygen plasma treatment.

2.1.1 | Isolation of primary rat hepatocytes and cell culture

Primary rat hepatocytes were freshly isolated from adult female Lewis rats (Charles River Laboratories, MA) according to the protocol #2011N000111 approved by the Institutional Animal Care and Use Committee (Dunn, Tompkins, & Yarmush, 1991; Seglen, 1976). Approximately $3.1\text{--}4.1 \times 10^4$ hepatocytes with 90–95% viability were cultured in the cell culture chamber of the device that was coated with 50 $\mu\text{g}/\text{ml}$ fibronectin (Sigma-Aldrich, St. Louis, MO) for 20–40 min at 37°C and 10% CO_2 as described previously (Kang et al., 2018; McCarty et al., 2016). The cells were seeded and cultured at 37°C and 10% CO_2 in Dulbecco's modified eagle's medium (DMEM; Life Technologies, Carlsbad, CA) supplemented with 10% fetal bovine serum (Sigma-Aldrich), 0.5 U/ml insulin, 7 ng/ml glucagon, 20 ng/ml epidermal growth factor, 7.5 $\mu\text{g}/\text{ml}$ hydrocortisone, 200 U/ml penicillin, 200 $\mu\text{g}/\text{ml}$ streptomycin, and 50 $\mu\text{g}/\text{ml}$ gentamycin.

2.2 | Generation of the oxygen gradient in the MPOC device

To create the oxygen gradient, sulfite and cobalt were used for removing oxygen and for accelerating oxygen depletion, respectively (Abudara, Jiang, & Eyzaguirre, 2002; Grasselli, Basini, Bussolati, & Bianco, 2005; Jiang et al., 2011; Shimizu et al., 1996). Oxygen-free media was prepared by dissolving 0.1 g sodium sulfite (Na_2SO_3) and 50 μl cobalt nitrate ($\text{Co}(\text{NO}_3)_2$) in 10 ml DMEM media to result in a final concentration of 1% sulfite and 100 μM cobalt in the media (GmbH, 2013). Oxygen-dissolved media was the DMEM media. DMEM media (one inlet) and DMEM supplemented with 1% sulfite and 100 μM cobalt (the other inlet) flew into the gradient generator of the device. The oxygen gradient generation was tested in the cell culture chamber of the device by mixing DMEM media (0% sulfite/0 μM cobalt) and DMEM supplemented with 1% sulfite and 100 μM cobalt at 30–120 $\mu\text{l}/\text{hr}$.

2.3 | Measurement of dissolved oxygen (DO) in aqueous solution

Solutions of different sulfite and cobalt concentrations, 0% sulfite/0 μM cobalt, 0.25% sulfite/25 μM cobalt, 0.5% sulfite/50 μM cobalt, 0.75% sulfite/75 μM cobalt, 1% sulfite/100 μM cobalt, 100 μM cobalt, 1% sulfite, and 95% N_2 /5% CO_2 in water, were prepared in 50 ml conical tubes. The DO level of each aqueous solution was measured by the DO meter (EW35643-14; Oakton DO6, Vernon Hills, IL) with an accuracy of $\pm 1.5\%$ of the full-scale range.

For detection of the oxygen levels in the MPOC device, the VisiSens system with a VisiSens 2D sensor film (PreSens/TD system GmbH, Germany) was used according to the manufacturer's instructions. The VisiSens sensor film was adhered to the glass microscope slide using super glue. The microfluidic device was attached to the VisiSens sensor film after oxygen plasma treatment. The oxygen level in the microfluidic device was detected by the

VisiSens system with a modular detector unit for 2D read-out of fluorescent oxygen sensor foils. Oxygen-sensing images were visualized by VisiSens AnalytiCal 1 software, followed by the quantification of the oxygen profile through the ImageJ software (NIH, Bethesda, MD).

2.4 | Perfusion of cells with the oxygen gradient

The device seeded with primary hepatocytes was connected to the perfusion system through Tygon tubing as described previously (Kang et al., 2018; McCarty et al., 2016). 20–24 hr after cell seeding, cells were perfused with the oxygen gradient generated by mixing DMEM media and DMEM supplemented with 1% sulfite and 100 μM cobalt at 120 $\mu\text{l}/\text{hr}$ for 2 hr.

2.4.1 | Immunofluorescence assay

Following the oxygen gradient exposure, the microfluidic device was detached from the perfusion system. Cells were fixed with 4% paraformaldehyde for 15 min at room temperature. We then cut around the pattern of the culture chamber of the PDMS layer on the surface of the glass microscope slide with a razor blade. The PDMS layer was peeled off from the glass microscope slide while cells were still attached to the glass slide. Next, the cells were incubated with 0.25% Triton X-100 in phosphate-buffered saline (PBS) for 10 min, followed by incubation with 1% bovine serum albumin (BSA) and 22.52 mg/ml glycine in PBST (PBS + 0.1% Tween 20) for 30 min to block unspecific binding of antibodies. Cells were then incubated overnight at 4°C with the diluted primary antibody solution in 1% BSA in PBST. HIF1 α antibody (anti-HIF1 α , mouse monoclonal antibody, 1:50, NB100–105; Novus Biologicals, Littleton, CO) and hypoxyprome ATTO 594 (1:100, mouse monoclonal antibody conjugated to ATTO 594 fluorophore; Hypoxyprome, Burlington, MA) were used to detect pimonidazole adducts in hypoxic cells. The next day, cells were incubated with goat antimouse conjugated secondary antibody (Texas Red, 1:1,000, ab6787; Abcam, Cambridge, MA) in 1% BSA for 1 hr at room temperature in the dark. Cell nuclei were counterstained with Hoechst (1:2,000, 33258; Thermo Fisher Scientific). Images were obtained by the EVOS fluorescence microscope (EVOS FL; Thermo Fisher Scientific).

2.5 | Cell viability assay and detection of ROS

For cell viability analysis, cells in the device were stained with the live/dead cell assay kit (L3224; Thermo Fisher Scientific) or tetramethylrhodamine methyl ester (TMRM; 500 nM; Thermo Fisher Scientific) for 15–20 min at 37°C according to the manufacturer's instructions. For the detection of ROS, cells were stained with ROS detection reagent—CM-H2DCFDA (C6827; Thermo Fisher Scientific) according to the manufacturer's protocol. Cell nuclei were stained with Hoechst (33258; Thermo Fisher Scientific). Images were obtained using the EVOS fluorescence microscope. The average fluorescence intensity across the width of the device was quantified

using the ImageJ software. For the well plate experiments, PrestoBlue reagent (Thermo Fisher Scientific) was used according to the manufacturer's protocol.

2.5.1 | RNA isolation and RT-PCR analysis

Hepatocytes were harvested from each channel of the cell culture chamber after induction with the hypoxia gradient. Total RNA was isolated using RNA Microprep Kit (R1051; Zymo Research, Irvine, CA) following the manufacturer's protocol. Total RNA (10–100 ng) was used for complementary DNA (cDNA) synthesis using a commercially available cDNA synthesis kit (iScript; Bio-Rad, Portland, ME) following the instructions of the manufacturer. The synthesized cDNA was amplified with a real-time polymerase chain reaction (RT-PCR) system (ViiA 7; Life Technologies) using a Power SYBR Green PCR Master Mix Kit (Life Technologies) according to the manufacturer's instructions. The following PCR primer pair for the amplification of rat HIF1 α gene was used: 5'-GCGAGAACGAGAAGA AAAATAGGA-3' and 5'-GGGGAAGTGGCAACTGATGA-3'. The β -actin was used as an internal control and was amplified with the following primers: 5'-CCTGCCTTTGCCGATCC-3' and 5'-GCGCG GCGATATCATCATCC-3'. The following protocol was used for the thermal cycler: 50°C for 2 min, 95°C for 10 min, 42 cycles at 95°C for 14 s and 60°C for 1 min. The relative messenger RNA (mRNA) expression was quantified in duplicate using the comparative C_t ($\Delta\Delta C_t$) method on the ViiA 7 real-time PCR system.

2.6 | Image quantification

All fluorescent microscopy images of the stained cells were quantified using the built-in functions of the ImageJ software: conversion to greyscale, subtraction of the background, enhancement of the image contrast, and normalization of the average intensity. The average intensities (normalized against the minimum and maximum intensity of cell images) were rescaled to reflect percentages. All data were plotted via curve fitting using nonlinear regression analysis.

2.7 | Statistical analysis

The quantitative data are presented as the mean \pm standard error of the mean from three to ten devices ($n = 3-10$) and were assessed using one-way ANOVA and Tukey's test. The p values $<.05$ were considered to be statistically significant.

3 | RESULTS

In this study, we used our MPOC device as a progressive hypoxia-on-a-chip platform by creating an oxygen gradient of 0.3–6.9% via the use of chemical oxygen quenchers in a fully oxygenated media rather than generating the oxygen gradient with a nitrogen/carbon dioxide mixture. We first characterized the generated oxygen gradient in the

MPOC device. We then showed in tissue-culture plates that the chemicals, sulfite and cobalt, used to induce the oxygen gradient did not affect the cell viability directly. Upon establishing the safe ranges for the chemicals used, we investigated whether the established oxygen gradient, in the MPOC device, resulted in a hypoxia gradient in the primary rat hepatocytes by assessing cell viability, hypoxia-marker pimonidazole levels, ROS production, and HIF1 α expression in cells exposed to different oxygen concentrations. We note that similar oxygen gradients have been reported in the rat liver compared to the human liver (Allen et al., 2005; Kietzmann, 2017; Lauth, 2009; M, 1996; Martinez et al., 2008).

3.1 | Oxygen gradient generation in the MPOC device

There are two different methods to simulate hypoxic conditions: direct bubbling of gas of the desired composition (e.g., 95% N₂ and 5% CO₂; physically induced hypoxia) and using oxygen quenchers (chemically induced hypoxia; Jiang et al., 2011). Here, we used the latter, where gradients in sulfite and cobalt were utilized to gradually quench the oxygen and generate an oxygen gradient in the MPOC device (Abudara et al., 2002; Grasselli et al., 2005; Jiang et al., 2011; Shimizu et al., 1996). This approach reduces the complexity and footprint of the system by alleviating the need to use large gas tanks and their additional tubing and pumping requirements. To accomplish the chemical quenching approach and to assess the concentration range necessary for the MPOC device, we first measured the equilibrium oxygen concentration in solutions of 0% sulfite/0 μ M cobalt, 0.25% sulfite/25 μ M cobalt, 0.5% sulfite/50 μ M cobalt, 0.75% sulfite/75 μ M cobalt, 1% sulfite/100 μ M cobalt, 100 μ M cobalt, 1% sulfite, and 95% N₂/5% CO₂ using the DO meter (Table S1). Measured oxygen concentrations decreased from 15.9% to 0% as the concentrations of sulfite and cobalt increased from 0% sulfite/0 μ M cobalt to 1% sulfite/100 μ M cobalt (Figure 2a). Moderate hypoxia of 1–3% O₂ was generated in the solution of 0.25% sulfite/25 μ M cobalt and 0.5% sulfite/50 μ M cobalt. The solution of 1% sulfite generated severe hypoxia of 0% oxygen while the solution of 100 μ M cobalt maintained an oxygen level of approximately 14.8%. These results are in accordance with the fact that sulfite plays a significant role in oxygen removal, and cobalt acts as a metal chelator to prevent cytotoxicity of sulfite (Zhongbao; & Jingqi, 2002).

Based on these results, we selected 1% sulfite/100 μ M cobalt as the extreme input for the creation of the oxygen gradient in the MPOC device to capture both severe and mild hypoxia as well as normoxia. We simulated the concentration gradient of sodium sulfite with a diffusion coefficient of 1.2×10^{-9} m²/s in water (Leaist, 1985) and a molecular weight of 126 Da at a flow rate of 30–120 μ l/hr in the MPOC device using COMSOL[®] Multiphysics (COMSOL Inc., Burlington, MA; Figure 2b). These simulations showed that we were able to establish well-separated compartments of different sodium sulfite concentrations using these flow parameters. We created the concentration gradient of sulfite and cobalt in the MPOC device by mixing cell culture media—DMEM and DMEM media supplemented

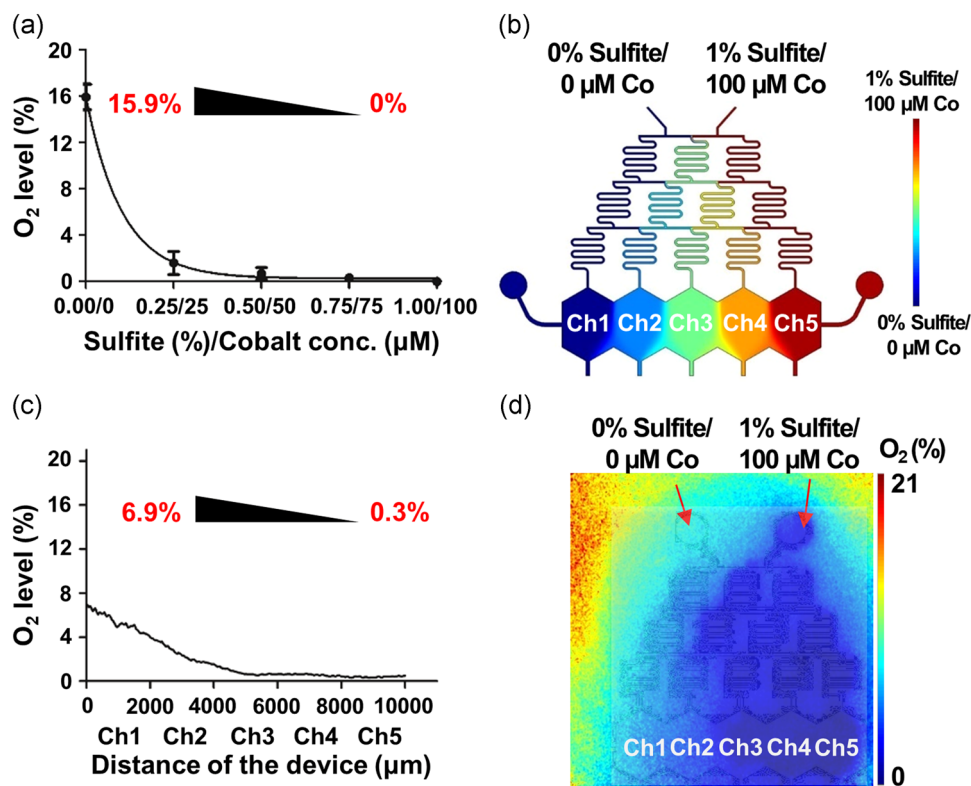


FIGURE 2 Oxygen gradient in the MPOC device. (a) The plot of measured oxygen levels versus varying sulfite and cobalt concentrations in water where an oxygen range of 15.9–0% was measured. The measurements were performed in 50 ml conical tubes. (b) Simulation of the oxygen gradient by COMSOL Multiphysics. (c) Plotted steady-state oxygen gradient profile of the MPOC device after perfusion with 0% sulfite/0 μM cobalt and 1% sulfite/100 μM cobalt, showing a gradient of 6.9–0.3% O₂. (d) Representative image of oxygen concentration distribution in the MPOC device measured by the Presens system. Inlet 1: 0% sulfite/0 μM cobalt and Inlet 2: 1% sulfite/100 μM cobalt. All data were obtained from at least three different experiments. MPOC, Metabolic Patterning on a Chip [Color figure can be viewed at wileyonlinelibrary.com]

with 1% sulfite and 100 μM cobalt via the gradient generator with a flow rate of 120 μl/hr under cell-free condition. The two extreme inlets of the gradient generator are shown in Figure 2b: 0% sulfite/0 μM cobalt and 1% sulfite/100 μM cobalt, corresponding to 15.9% and 0% oxygen, respectively. We detected the oxygen gradient along the width of the device via the oxygen-sensing VisiSens system (PreSens/TD system; GmbH, Germany; Figure S1). A descending oxygen concentration profile across the cell culture chamber was obtained along the ascending gradient of sulfite and cobalt (Figure 2c,d). The oxygen level in Channel 1, which was perfused with 0% sulfite/0 μM cobalt solution, was approximately 6.9%, while the oxygen level in Channel 5, which was perfused with 1% sulfite/100 μM cobalt solution, was approximately 0.3%.

3.1.1 | Cytotoxicity of sulfite and cobalt in well plate hepatocyte cultures

We then investigated the cytotoxicity of sulfite and cobalt and assessed the viability of hepatocytes incubated with these chemicals in tissue-culture plates before conducting experiments in the MPOC device. Primary rat hepatocytes cultured in well plates were treated with media containing different concentrations of sulfite and cobalt

and with 95% N₂/5% CO₂ (Supporting Information text, Figure S2). The results showed that the 1% sulfite/100 μM cobalt media, which was used for oxygen gradient generation in the MPOC device, did not result in significant toxicity for the first 2 hr, which is the time frame for the rest of the experiments conducted in this study.

3.2 | Confirmation of the hypoxia gradient in hepatocytes in response to the oxygen gradient in the MPOC device

Pimonidazole is a common hypoxia marker that is reductively activated in hypoxic cells and forms adducts via stable covalent bonding with thiol-containing proteins (Aguilera & Brekken, 2014). Hypoxic cells can then be recognized via immunohistochemical detection of this hypoxia marker. To confirm that we can indeed establish intracellular hypoxia in a gradual fashion in the MPOC device, we quantified the presence of pimonidazole adducts in hepatocytes upon oxygen gradient exposure. Primary rat hepatocytes were perfused with the media containing the oxygen quenchers supplemented with 200 μM pimonidazole hydrochloride at a flow rate of 120 μl/hr for 2 hr. After exposing cells to the oxygen gradient, we stained pimonidazole adducts with hypoxyprobe ATTO 594 and

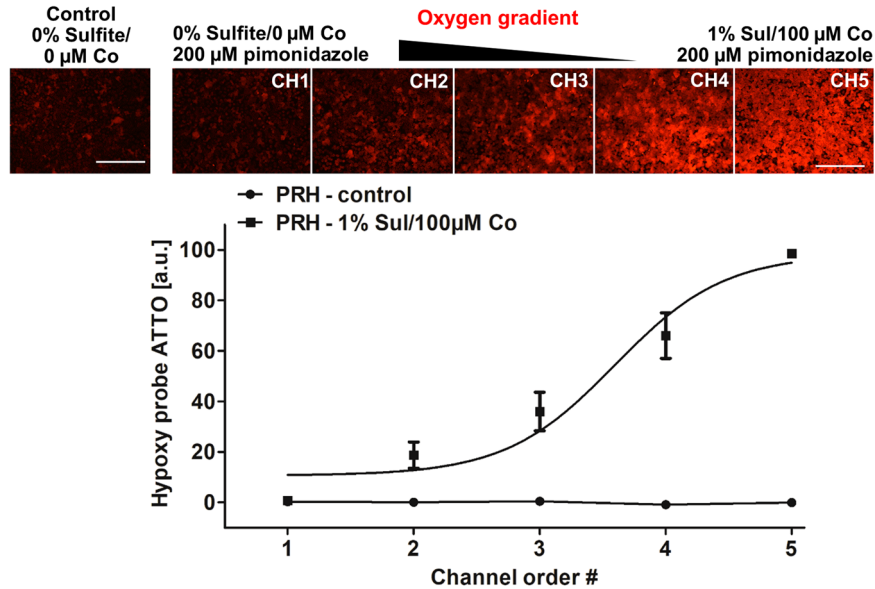


FIGURE 3 Hypoxia gradient in primary rat hepatocytes in the MPOC device. Hepatocytes cultured in the MPOC device were perfused with media supplemented with 200 μM pimonidazole and were exposed to the oxygen gradient created by 0% sulfite/0 μM cobalt and 1% sulfite/100 μM cobalt for 2 hr. The control group consisted of cells perfused with DMEM media only. Afterward, cells were stained with hypoxyprobe ATTO 594 to detect the by-product of pimonidazole. An increasing gradient of hypoxyprobe ATTO 594 was observed along the decreasing oxygen gradient across the width of the device. Image quantification for hypoxyprobe ATTO 594 staining was performed via the ImageJ software. All data met $p < .05$ except that control versus Channels 1 and 2; Channel 1 versus Channel 2; and Channel 2 versus Channel 3 are not significant (one-way ANOVA $n = 6$, Tukey's test). The data point of Channel 1 in the experiment of the oxygen gradient is similar to that of Channel 1 in the control experiment in the graph. Scale bar: 400 μm . ANOVA, analysis of variance; DMEM, Dulbecco's modified eagle's medium; MPOC, Metabolic Patterning on a Chip [Color figure can be viewed at wileyonlinelibrary.com]

observed an increasing gradient of the stain across the width of the device (Figure 3). Hepatocytes in Channel 1, perfused at an oxygen concentration of 6.9%, displayed low fluorescence intensity, similar to that of the control group (perfused with DMEM media only). In contrast, hepatocytes in Channel 5, perfused at an oxygen concentration of 0.3%, displayed high fluorescence intensity indicating high levels of intracellular hypoxia.

3.3 | Cell viability of hepatocytes cultured in the MPOC device

After confirming the intracellular hypoxia patterning of hepatocytes, we investigated cell viability in response to the oxygen gradient in the MPOC device. Similar to previous experiments, hepatocytes were perfused with varying amounts of oxygen quenchers for 2 hr. Cell viability was analyzed by staining the cells with the live/dead assay kit and TMRM reagent, as described in Section 2. Ethidium homodimer-1 staining demonstrated that most cells remained viable in Channel 1, where hepatocytes were cultured at 6.9% O_2 , similar to that of the control group perfused with DMEM media only (Figure 4a). In contrast, the cell viability of hepatocytes decreased to approximately 80% in Channel 5, where hepatocytes were exposed to 0.3% O_2 . In addition, the activities of both esterase, responsible for the hydrolysis of Calcein-AM, and the mitochondrial membrane potential, an indicator of cell viability and metabolism, were decreased to approximately 40–50% along with the oxygen gradient (Figure 4b). Cell viability of hepatocytes under the

hypoxia gradient in the MPOC can be affected by cells in the neighboring channels. The MPOC device was specifically designed to allow for such interactions that draw upon the continuous nature of the tissue and gradients in the liver sinusoid in vivo. For instance, the loss of cell viability in Channel 5 could negatively affect the cell viability of the neighboring channel. On the other hand, cells in the normoxic Channel 1 might have a positive paracrine effect on cells in the neighboring hypoxia channel.

3.4 | ROS production of hepatocytes in response to the oxygen gradient in the MPOC device

The cell viability loss caused by low oxygen concentration in the liver is associated with the generation of ROS (Busek, Stefan, Steege, Klotzbach, & Sonntag, 2016; Eltzschig & Eckle, 2011; Hockel & Vaupel, 2001). Particularly, these species are involved in key mechanisms leading to cell dysfunction and death under hypoxic conditions. ROS can be accumulated in hypoxic hepatocytes, unlike normal cells due to the imbalance of ROS production and removal towards the pro-oxidative state (Jaeschke, 2000). We investigated ROS accumulation in response to the applied oxygen gradient. Following the perfusion in the MPOC device, primary rat hepatocytes were stained with ROS detection reagent CM-H2DCFDA. The highest ROS production was observed in Channel 5 where the hepatocytes were exposed to severe hypoxia. The lowest expression levels were observed in Channel 1, where cells were cultured under normoxic conditions (Figure 5). Image quantification of ROS staining

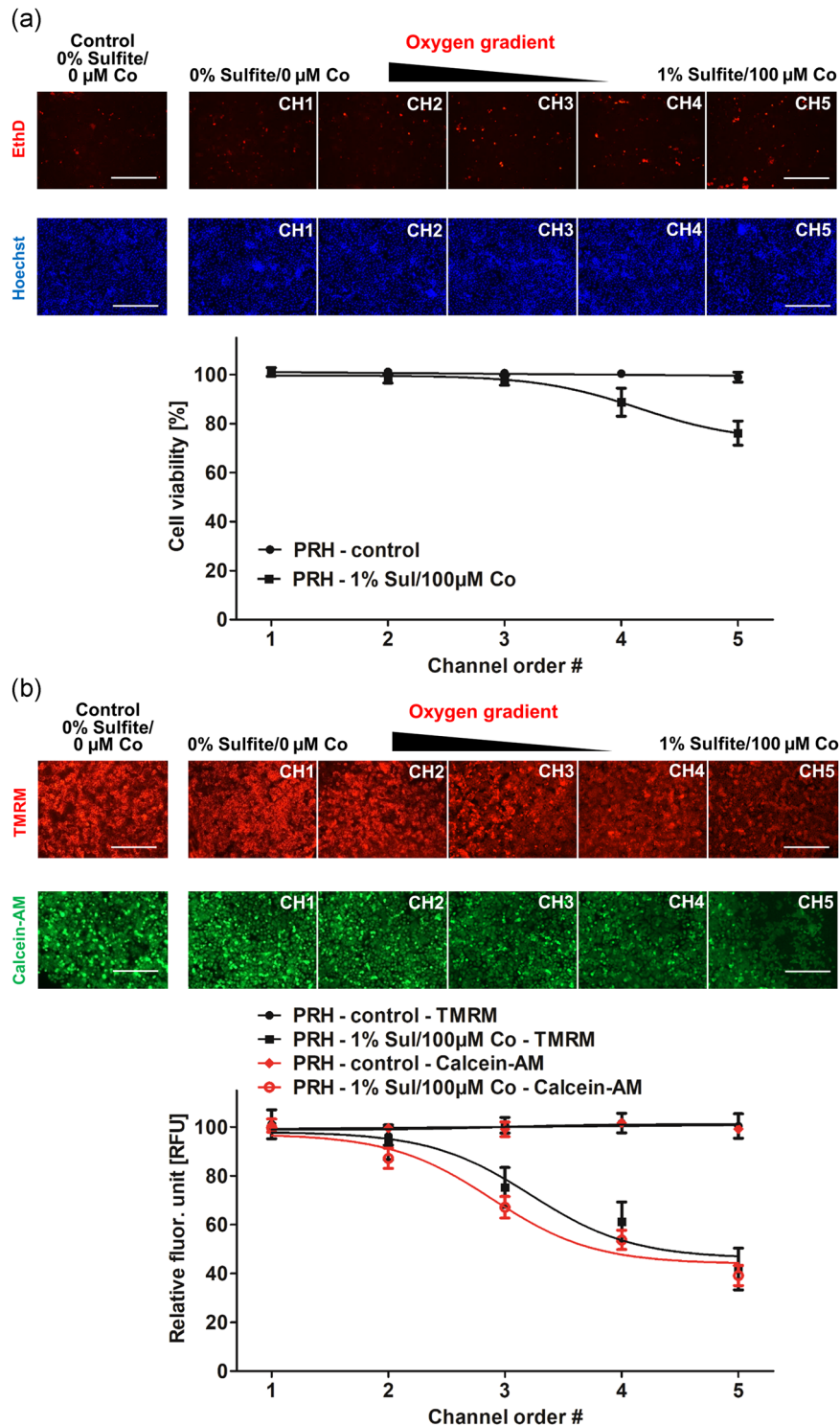


FIGURE 4 Cell viability of primary rat hepatocytes in the MPOC device. Hepatocytes cultured in the MPOC device were exposed to an oxygen gradient created by 0% sulfite/0 μM cobalt and 1% sulfite/100 μM cobalt for 2 hr. Control groups consisted of cells perfused with DMEM media only. Afterward, cells were stained with (a) EthD and Hoechst to assess cell viability. The cell viability of hepatocytes was decreased to approximately 80% along the hypoxia gradient across the width of the device, while hepatocytes in the control group (perfused with oxygen-dissolved DMEM media) remained viable. Image quantification was performed via the ImageJ software. All data met $p < .05$ except that control versus Channels 1, 2, and 3; Channel 1 versus Channels 2, 3, and 4; Channel 2 versus Channels 3 and 4; Channel 3 versus Channel 4; and Channel 4 versus Channel 5 are not significant (one-way ANOVA $n = 5$, Tukey's test). Scale bar: 400 μm . (b) TMRM and calcein staining. The metabolic activity was decreased along the hypoxia gradient. Image quantification was performed via the ImageJ software. For the TMRM staining, all data met $p < .05$ except that control versus Channels 1, 2, and 3; Channel 1 versus Channels 2 and 3; Channel 2 versus Channel 3; Channel 3 versus Channel 4; and Channel 4 versus Channel 5 are not significant (one-way ANOVA $n = 6$, Tukey's test). For the calcein staining, all data met $p < .05$ except that control versus Channels 1 and 2; Channel 1 versus Channel 2; Channel 3 versus Channel 4; and Channel 4 versus Channel 5 are not significant (one-way ANOVA $n = 6$, Tukey's test). Scale bar: 400 μm . ANOVA, analysis of variance; DMEM, Dulbecco's modified eagle's medium; MPOC, Metabolic Patterning on a Chip [Color figure can be viewed at wileyonlinelibrary.com]

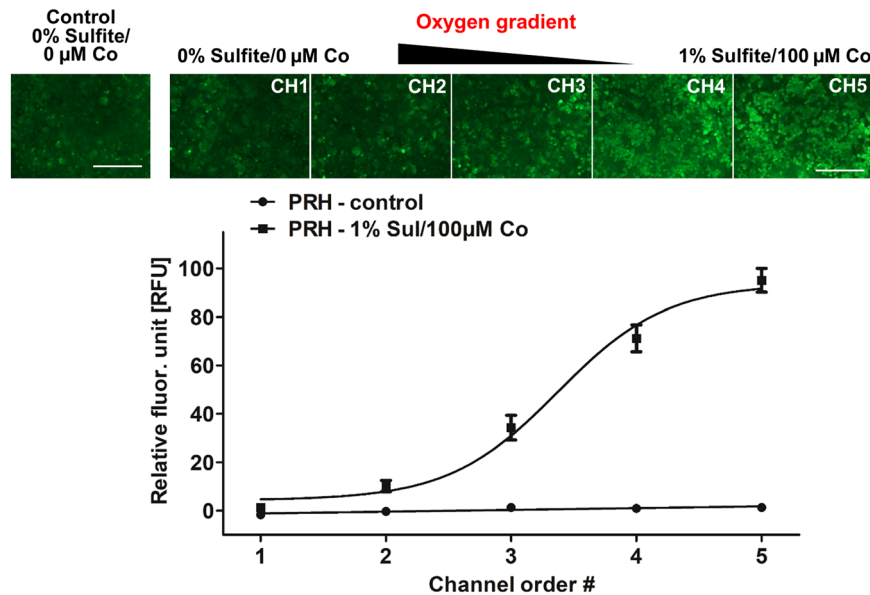


FIGURE 5 ROS generation of primary rat hepatocytes in response to the hypoxia gradient in the MPOC device. Following perfusion with the oxygen gradient generated by 0% sulfite/0 μM cobalt and 1% sulfite/100 μM cobalt, cells were stained with CM-H2DCFDA to detect ROS levels. An increasing pattern of ROS accumulation was observed along the hypoxia gradient across the width of the device. Control groups consisted of cells perfused with DMEM media only. Image quantification was performed using ImageJ software. All data met $p < .05$ except that control versus Channel 1; and Channel 1 versus Channel 2 are not significant (one-way ANOVA $n = 10$, Tukey's test). Scale bar: 400 μm . ANOVA, analysis of variance; DMEM, Dulbecco's modified eagle's medium; MPOC, Metabolic Patterning on a Chip; ROS, reactive oxygen species [Color figure can be viewed at wileyonlinelibrary.com]

demonstrated an ascending gradient profile of ROS generation across the width of the device.

3.5 | HIF1 α expression profile of hepatocytes in response to the oxygen gradient

The ROS generation in hypoxic cells triggers the activation of HIF- α s, which are the key mediators of cell survival. In hypoxic tissue, they regulate numerous genes associated with cellular adaptations to hypoxia, whereas in the normal tissue, these factors are degraded by the Von Hippel-Lindau protein and proteasomes (Covello et al., 2006; Das et al., 2008; Keith et al., 2011; Moreno-Manzano et al., 2010).

We investigated HIF1 α expression in primary rat hepatocytes in response to the generated oxygen gradient. After the perfusion in the MPOC device, we stained the cells with HIF1 α antibody and observed a slightly ascending gradient of HIF1 α across the width of the device (Figure 6a). Hepatocytes in Channel 5, exposed to severe hypoxia, displayed a higher fluorescence intensity compared to that of hepatocytes in Channel 1. We then quantified the mRNA expression of HIF1 α via RT-PCR after collecting the cells from each channel of the cell culture chamber of the MPOC device. Similar to the HIF1 α antibody staining, hepatocytes exposed to severe hypoxia revealed higher HIF1 α mRNA expression levels along the increasing hypoxia gradient (Figure 6b). Compared to cells in Channel 1, cultured under normoxic conditions, an approximately 3-fold increase in HIF1 α mRNA levels was observed in cells cultured under hypoxic conditions in Channel 5.

4 | DISCUSSION

Previously, we introduced the MPOC device capable of creating metabolic patterns in a microfluidic platform via actively enforced concentration gradients of different inducers. Here, we used this device to establish an in vitro microfluidic hypoxia model that can capture a broad range of oxygen concentrations from the physiologically relevant normoxia to severe hypoxia. The MPOC device was perfused with 0% sulfite/0 μM cobalt and 1% sulfite/100 μM cobalt solutions to generate a chemically induced oxygen gradient in the target range of 0–15.9%. On the other hand, direct oxygen measurements in the MPOC device showed that an oxygen gradient of 0.3–6.9% was achieved (Figure 2). This result suggests that the explicit characterization of the oxygen gradient in the MPOC device is critical for the interpretation of our results. The simple predictions of flow simulations combined with the use of oxygen measurements of sulfite/cobalt mixtures in stationary well-equilibrated solutions did not translate to our measurements in the device. We hypothesize that this discrepancy could be a result of (a) different measurement methods and the lack of measurement resolution in smaller footprint devices such as ours but more so; (b) rapid oxygen diffusion and high sulfite/cobalt concentration channels acting as oxygen sinks for the overall device as follows. Oxygen (16 Da) is smaller in size than sulfite (126 Da), resulting in a larger diffusion coefficient. Thus, oxygen could easily diffuse from one channel to the next, subsequently getting quenched by the sulfite, a very potent quencher of oxygen, leading to a decrease in overall oxygen concentration. The fifth channel perfused with 1% sulfite/100 μM cobalt might have become a sink for the

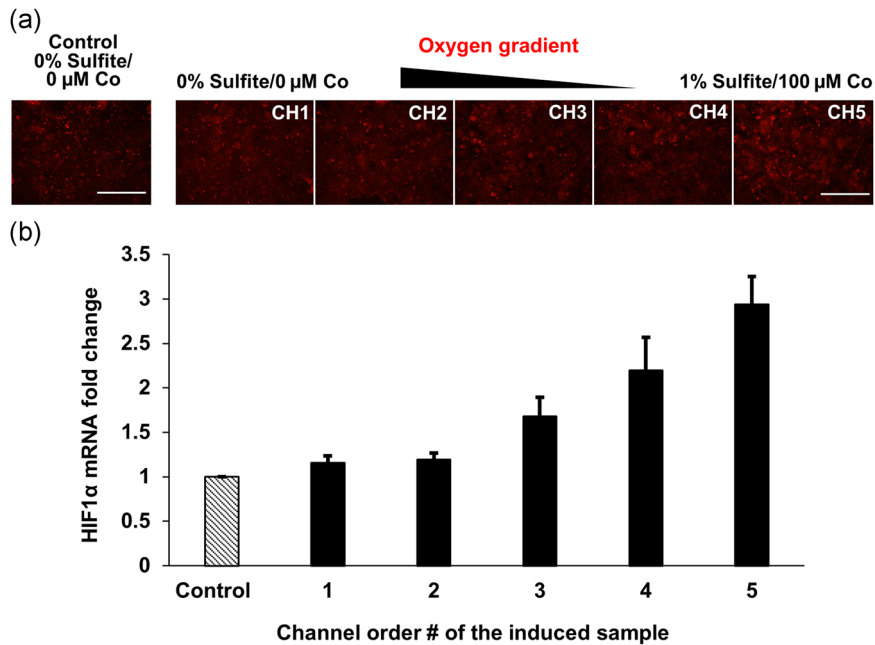


FIGURE 6 HIF1 α expression of primary rat hepatocytes in response to the hypoxia gradient in the MPOC device. (a) Hepatocytes cultured in the microfluidic device were exposed to the oxygen gradient created by 0% sulfite/0 μ M cobalt and 1% sulfite/100 μ M cobalt for 2 hr. Cells were stained with HIF1 α antibody following the perfusion. HIF1 α expression was slightly increased along the increasing hypoxia gradient across the width of the device. (b) HIF1 α mRNA levels were quantified via RT-PCR analysis after inducing hepatocytes with the oxygen gradient created by two different concentrations of sulfite/cobalt for 2 hr. An ascending gradient of HIF1 α mRNA fold change was obtained along with the width of the device. The control group was cultured with 0% sulfite/0 μ M cobalt. All data met $p < .05$ except that control versus Channels 1, 2, and 3; Channel 1 versus Channels 2 and 3; Channel 2 versus Channel 3; Channel 3 versus Channel 4; and Channel 4 versus Channel 5 are not significant (one-way ANOVA $n = 6$, Tukey's test). Scale bar: 400 μ m. ANOVA, analysis of variance; HIF, hypoxia-inducible factor; MPOC, Metabolic Patterning on a Chip; mRNA, messenger RNA [Color figure can be viewed at wileyonlinelibrary.com]

whole system, resulting in a global quenching effect rather than a local and channel-specific one. Nevertheless, the established oxygen gradient of 0.3–6.9% is a unique normoxia-hypoxia gradient model, capturing both the physiologically relevant oxygen levels along the liver sinusoid and the hypoxic conditions in the liver ischemia. The pimonidazole staining further demonstrated that we successfully created an intracellular hypoxia gradient along the width of the cell culture chamber, where hepatocytes exhibited increasing levels of hypoxia with decreasing concentrations of oxygen. As shown in Figure 3, hepatocytes exposed to severely oxygen-depleted media became hypoxic cells (e.g., cells in Channels 4 and 5) while hepatocytes exposed to physiologically relevant oxygen levels did not exhibit a statistically significant difference in their amount of pimonidazole (e.g., Channels 1 and 2) compared to the control group.

As the next step, we assessed cell viability and metabolism. Along the oxygen gradient of 6.9–0.3%, the cell viability, and metabolic activity decreased to 80% and 40–50%, respectively (Figure 4). Considering that the mitochondrial activity depends on oxygen availability, the decrease in TMRM accumulation is well understood. Thus, oxygen deprivation and severe hypoxia impaired the metabolic activity of the cells, even though its effect on cell viability was less drastic. In addition, the reduced oxygen concentration induces the generation of ROS such as superoxide, hydrogen peroxide, hydroxyl radical, hydroxyl ion, and nitric oxide which are by-products of mitochondrial electron transport chain (Hancock, Desikan, & Neill,

2001). Their accumulation causes toxicity and cellular DNA damage through oxidative stress, which eventually results in apoptosis. Quantification of ROS accumulation in response to the oxygen gradient in the MPOC device indicated that hepatocytes exposed to severe hypoxia generated high levels of ROS due to increased oxidative stress, while hepatocytes exposed to normoxia exhibited less oxidative stress (Figure 5). Under severe hypoxic conditions, the cells die because of excessive ROS generation, which correlated well with the 20% decrease of cell viability and up to 50% reduction in mitochondrial and esterase activities in Channel 5 perfused with an oxygen concentration of 0.3%. HIFs are involved in the metabolic adaptation of ischemic tissues to maintain cellular viability for a longer period. In the MPOC device, HIF1 α expression was significantly upregulated in the hypoxic microenvironment (Figure 6). The ascending trend of HIF1 α expression of hepatocytes in response to the increasing hypoxia gradient exhibits a close correlation with the increasing ROS accumulation. Low oxygen levels cause ROS generation in the cells, resulting in oxidative stress, and they trigger HIF α activation to adapt to the abnormal environment as in the case of severe hypoxia and ischemia.

These results demonstrate that we established a progressive hypoxia-on-a-chip platform, where an oxygen gradient of 0.3–6.9% was generated, capturing a wide range of physiologically relevant oxygen concentrations, ranging from normoxia to severe hypoxia. We showed the applicability of this platform by confirming intracellular

hypoxia establishment in hepatocytes, by evaluating cell viability and metabolic activity, and by demonstrating the regulation of hypoxia-associated factors, ROS, and HIFs in response to the applied oxygen gradient. This progressive hypoxia model can be further used to study the mechanisms and regulations of these factors in hypoxia-associated liver diseases. Furthermore, it can be utilized in studies of other disease models such as NAFLD where carbohydrate and lipid metabolisms are heavily reliant on the availability of oxygen. Specifically, the lower concentrations of oxygen is hypothesized to result in more drastic fat accumulation (Schleicher, Dahmen, Guthke, & Schuster, 2017). Accordingly, this device could potentially be employed to understand the relation between oxygen deprivation and fat accumulation in hepatocytes.

5 | CONCLUSIONS

In this study, we built upon our recent MPOC device to create a progressive hypoxia on-a-chip platform. In this platform, primary rat hepatocytes were perfused with two extreme inlets of 0% sulfite/0 μ M cobalt and 1% sulfite/100 μ M cobalt to create an oxygen gradient of 0.3–6.9%. This range captures both physiologically relevant normal zonal conditions and severely hypoxic conditions relevant for injury and disease conditions. The cell viability of hepatocytes in response to the hypoxia gradient decreased to approximately 80% along the increasing hypoxia gradient. Increasing levels for the hypoxia-marker pimonidazole, ROS accumulation, and HIF expression were established along the descending oxygen gradient. These results demonstrated that our platform was able to replicate the distinct metabolic activities of hepatocytes exposed to oxygen gradients, mimicking the normal physiology as well as the pathological state of injured liver tissue. As such, this platform could be used for the study of various aspects of liver physiology, including the role of oxygen and hypoxia-associated mechanisms in healthy liver and liver diseases, in addition to the study of drug toxicity and efficacy under oxygen-limited conditions, specifically the efficacy of hypoxia-activated prodrugs that are activated in the hypoxia microenvironment (Hunter, Wouters, & Wilson, 2016). While we have studied short-term responses to oxygen gradients in this work, our ultimate goal is to use the MPOC device to study the long-term effects of oxygen gradients on fully recapitulated liver tissues with multiple cell types combining our approach here with previous long-term microfluidic hepatic culture and coculture models from our lab (McCarty et al., 2014; Prodanov et al., 2016).

Beyond liver and hypoxia-associated liver diseases, varying levels of hypoxic microenvironments are also observed in other tissues such as solid tumors and wound tissues (Kim et al., 2018; McKeown, 2014; Reichner & Albina, 2004; Samanta, Gilkes, Chaturvedi, Xiang, & Semenza, 2014; Sen, 2009). Low oxygen concentration and poor oxygen delivery to the tissue result in abnormal cellular metabolism and function; and can lead to poor therapy response to cancer treatment, delay of wound healing, and inflammation (Kim et al., 2018; Reichner & Albina, 2004; Sen, 2009). The advancement of in

vitro platforms, that are capable of simulating various oxygenation conditions simultaneously, can facilitate and accelerate research on the role of hypoxia in these tissues and possible remedies for the adverse outcomes due to hypoxia. Our progressive hypoxia-on-a-chip model, as presented here, can be used as a platform (a) to understand the role of hypoxia-associated factors in physiological and pathophysiological state of the liver; (b) to investigate other disease models such as NAFLD where oxidative stress plays a role in disease progression as we have recently demonstrated (Bulutoglu et al., 2019); (c) to study the complexity and heterogeneity of tissue healing and therapy processes; and (d) to assess the safety and efficacy of new drugs for clinical use in a reproducible manner.

ACKNOWLEDGMENTS

This research was supported by grants from the National Institutes of Health (NIH# 1R21EB020192, NIH# 5R01EB023812, NIH #1F32EB026916 and NIH# 5P41EB002503) and Shriners Hospitals for Children (# 84311, Nano-Micro Core Special Shared Facility and Shriners Morphology and Image Analysis Special Shared Facility). We gratefully acknowledge the work of Peony Banik and Sonal Nagpal for liver cell isolation through the Cell Resource Core at the Massachusetts General Hospital.

CONFLICT OF INTERESTS

The authors declare that there are no conflict of interests.

REFERENCES

- Abudara, V., Jiang, R. G., & Eyzaguirre, C. (2002). Behavior of junction channels between rat glomus cells during normoxia and hypoxia. *Journal of Neurophysiology*, 88(2), 639–649.
- Aguilera, K. Y., & Brekken, R. A. (2014). Hypoxia studies with pimonidazole in vivo. *Bio-Protocol*, 4(19), e1254.
- Albillos, A., Lario, M., & Alvarez-Mon, M. (2014). Cirrhosis-associated immune dysfunction: Distinctive features and clinical relevance. *Journal of Hepatology*, 61(6), 1385–1396. <https://doi.org/10.1016/j.jhep.2014.08.010>
- Allen, J. W., Khetani, S. R., & Bhatia, S. N. (2005). In vitro zonation and toxicity in a hepatocyte bioreactor. *Toxicological Sciences*, 84(1), 110–119. <https://doi.org/10.1093/toxsci/kfi052>
- Anada, T., Fukuda, J., Sai, Y., & Suzuki, O. (2012). An oxygen-permeable spheroid culture system for the prevention of central hypoxia and necrosis of spheroids. *Biomaterials*, 33(33), 8430–8441. <https://doi.org/10.1016/j.biomaterials.2012.08.040>
- Berndt, N., & Holzthutter, H. G. (2018). Dynamic metabolic zonation of the hepatic glucose metabolism is accomplished by sinusoidal plasma gradients of nutrients and hormones. *Frontiers in Physiology*, 9, 1786. <https://doi.org/10.3389/fphys.2018.01786>

- Brooks, A. J., Eastwood, J., Beckingham, I. J., & Girling, K. J. (2004). Liver tissue partial pressure of oxygen and carbon dioxide during partial hepatectomy. *British Journal of Anaesthesia*, 92(5), 735–737. <https://doi.org/10.1093/bja/ae112>
- Brooks, A. J., Hammond, J. S., Girling, K., & Beckingham, I. J. (2007). The effect of hepatic vascular inflow occlusion on liver tissue pH, carbon dioxide, and oxygen partial pressures: Defining the optimal clamp/release regime for intermittent portal clamping. *Journal of Surgical Research*, 141(2), 247–251. <https://doi.org/10.1016/j.jss.2006.10.054>
- Bulutoglu, B., Rey-Bedon, C., Kang, Y. B. A., Mert, S., Yarmush, M. L., & Usta, O. B. (2019). A microfluidic patterned model of nonalcoholic fatty liver disease: Applications to disease progression and zonation. *Lab on a Chip*, 19(18), 3022–3031. <https://doi.org/10.1039/c9lc00354a>
- Busek, M. G., Stefan, Steege, T., Klotzbach, U., & Sonntag, F. (2016). Generating hypoxic conditions in microfluidic cell culture systems. *Current Directions in Biomedical Engineering*, 2(1), 5.
- Camp, J. P., & Capitano, A. T. (2007). Induction of zone-like liver function gradients in HepG2 cells by varying culture medium height. *Biotechnology Progress*, 23(6), 1485–1491. <https://doi.org/10.1021/bp070308v>
- Carreau, A., El Hafny-Rahbi, B., Matejuk, A., Grillon, C., & Kieda, C. (2011). Why is the partial oxygen pressure of human tissues a crucial parameter? Small molecules and hypoxia. *Journal of Cellular and Molecular Medicine*, 15(6), 1239–1253. <https://doi.org/10.1111/j.1582-4934.2011.01258.x>
- Cassim, S., Raymond, V. A., Lapierre, P., & Bilodeau, M. (2017). From in vivo to in vitro: Major metabolic alterations take place in hepatocytes during and following isolation. *PLoS One*, 12(12):e0190366. <https://doi.org/10.1371/journal.pone.0190366>
- Castilla, D. M., Liu, Z. J., & Velazquez, O. C. (2012). Oxygen: Implications for wound healing. *Advances in Wound Care*, 1(6), 225–230. <https://doi.org/10.1089/wound.2011.0319>
- Chang, C. W., Cheng, Y. J., Tu, M., Chen, Y. H., Peng, C. C., Liao, W. H., & Tung, Y. C. (2014). A polydimethylsiloxane-polycarbonate hybrid microfluidic device capable of generating perpendicular chemical and oxygen gradients for cell culture studies. *Lab on a Chip*, 14(19), 3762–3772. <https://doi.org/10.1039/c4lc00732h>
- Cho, C. H., Park, J., Nagrath, D., Tilles, A. W., Berthiaume, F., Toner, M., & Yarmush, M. L. (2007). Oxygen uptake rates and liver-specific functions of hepatocyte and 3T3 fibroblast cocultures. *Biotechnology and Bioengineering*, 97(1), 188–199. <https://doi.org/10.1002/bit.21225>
- Copple, B. L. (2010). Hypoxia stimulates hepatocyte epithelial to mesenchymal transition by hypoxia-inducible factor and transforming growth factor- β -dependent mechanisms. *Liver International*, 30(5), 669–682. <https://doi.org/10.1111/j.1478-3231.2010.02205.x>
- Covello, K. L., Kehler, J., Yu, H., Gordan, J. D., Arsham, A. M., Hu, C. J., ... Keith, B. (2006). HIF-2 regulates Oct-4: Effects of hypoxia on stem cell function, embryonic development, and tumor growth. *Genes & Development*, 20(5), 557–570. <https://doi.org/10.1101/gad.1399906>
- Das, B., Tsuchida, R., Malkin, D., Koren, G., Baruchel, S., & Yeger, H. (2008). Hypoxia enhances tumor stemness by increasing the invasive and tumorigenic side population fraction. *Stem Cells*, 26(7), 1818–1830. <https://doi.org/10.1634/stemcells.2007-07242007-0724>, [pii].
- Dunn, J. C., Tompkins, R. G., & Yarmush, M. L. (1991). Long-term in vitro function of adult hepatocytes in a collagen sandwich configuration. *Biotechnology Progress*, 7(3), 237–245. <https://doi.org/10.1021/bp00009a007>
- Ebert, E. C. (2006). Hypoxic liver injury. *Mayo Clinic Proceedings*, 81(9), 1232–1236. <https://doi.org/10.4065/81.9.1232>
- Eltzschig, H. K., & Eckle, T. (2011). Ischemia and reperfusion—from mechanism to translation. *Nature Medicine*, 17(11), 1391–1401. <https://doi.org/10.1038/nm.2507>
- GmbH, P. P. S. (2013). *Oxygen Sensor Foils for Imaging SF-RPSu4*: PreSens.
- Grasselli, F., Basini, G., Bussolati, S., & Bianco, F. (2005). Cobalt chloride, a hypoxia-mimicking agent, modulates redox status and functional parameters of cultured swine granulosa cells. *Reproduction, Fertility, and Development*, 17(7), 715–720.
- Hall, Z., Bond, N. J., Ashmore, T., Sanders, F., Ament, Z., Wang, X., ... Griffin, J. L. (2017). Lipid zonation and phospholipid remodeling in nonalcoholic fatty liver disease. *Hepatology*, 65(4), 1165–1180. <https://doi.org/10.1002/hep.28953>
- Hancock, J. T., Desikan, R., & Neill, S. J. (2001). Role of reactive oxygen species in cell signalling pathways. *Biochemical Society Transactions*, 29(Pt 2), 345–349.
- Hockel, M., & Vaupel, P. (2001). Tumor hypoxia: Definitions and current clinical, biologic, and molecular aspects. *JNCI Journal of the National Cancer Institute*, 93(4), 266–276.
- Hunter, F. W., Wouters, B. G., & Wilson, W. R. (2016). Hypoxia-activated prodrugs: Paths forward in the era of personalised medicine. *British Journal of Cancer*, 114(10), 1071–1077. <https://doi.org/10.1038/bjc.2016.79>
- Jaeschke, H. (2000). Reactive oxygen and mechanisms of inflammatory liver injury. *Journal of Gastroenterology and Hepatology*, 15(7), 718–724.
- Jaeschke, H. (2011). Reactive oxygen and mechanisms of inflammatory liver injury: Present concepts. *Journal of Gastroenterology and Hepatology*, 26(Suppl 1), 173–179. <https://doi.org/10.1111/j.1440-1746.2010.06592.x>
- Jiang, B., Ren, C., Li, Y., Lu, Y., Li, W., Wu, Y., ... Zhang, C. (2011). Sodium sulfite is a potential hypoxia inducer that mimics hypoxic stress in *Caenorhabditis elegans*. *JBIC, Journal of Biological Inorganic Chemistry*, 16(2), 267–274. <https://doi.org/10.1007/s00775-010-0723-1>
- Kang, Y. B. A., Eo, J., Mert, S., Yarmush, M. L., & Usta, O. B. (2018). Metabolic patterning on a chip: Towards in vitro liver zonation of primary rat and human hepatocytes. *Scientific Reports*, 8(8951), 8951. <https://doi.org/10.1038/s41598-018-27179-6>
- Keith, B., Johnson, R. S., & Simon, M. C. (2011). HIF1 α and HIF2 α : Sibling rivalry in hypoxic tumour growth and progression. *Nature Reviews Cancer*, 12(1), 9–22. <https://doi.org/10.1038/nrc3183>
- Kietzmann, T. (2017). Metabolic zonation of the liver: The oxygen gradient revisited. *Redox Biology*, 11, 622–630. <https://doi.org/10.1016/j.redox.2017.01.012>
- Kim, S. W., Kim, I. K., Ha, J. H., Yeo, C. D., Kang, H. H., Kim, J. W., & Lee, S. H. (2018). Normobaric hyperoxia inhibits the progression of lung cancer by inducing apoptosis. *Experimental Biology and Medicine (Maywood)*, 243(9), 739–748. <https://doi.org/10.1177/1535370218774737>
- Ko, J., Ahn, J., Kim, S., Lee, Y., Lee, J., Park, D., & Jeon, N. L. (2019). Tumor spheroid-on-a-chip: A standardized microfluidic culture platform for investigating tumor angiogenesis. *Lab on a Chip*, 19(17), 2822–2833. <https://doi.org/10.1039/c9lc00140a>
- Lautt, W. W. (2009). In *Hepatic Circulation: Physiology and Pathophysiology*. San Rafael (CA).
- Leaist, D. G. (1985). Moments analysis of restricted ternary diffusion: Sodium sulfite + sodium hydroxide + water. *Canadian Journal of Chemistry*, 63, 2933–2939.
- Lefere, S., Van Steenkiste, C., Verhelst, X., Van Vlierberghe, H., Devisscher, L., & Geerts, A. (2016). Hypoxia-regulated mechanisms in the pathogenesis of obesity and nonalcoholic fatty liver disease. *Cellular and Molecular Life Science*, 73(18), 3419–3431. <https://doi.org/10.1007/s00018-016-2222-1>
- Lo, J. F., Sinkala, E., & Eddington, D. T. (2010). Oxygen gradients for open well cellular cultures via microfluidic substrates. *Lab on a Chip*, 10(18), 2394–2401. <https://doi.org/10.1039/c004660d>
- M, G. R. A. B. (1996). Normal values for physiological parameters. In G. R. a. W. U. (Ed.), *Comprehensive Human Physiology*, (pp. 2427–2447). Berlin-Heidelberg: Springer Verlag.
- Martinez, I., Nedredal, G. I., Oie, C. I., Warren, A., Johansen, O., Le Couteur, D. G., & Smedsrod, B. (2008). The influence of oxygen tension on the structure and function of isolated liver sinusoidal endothelial cells. *Comparative Hepatology*, 7, 4. <https://doi.org/10.1186/1476-5926-7-4>

- McCarty, W. J., Usta, O. B., Luitje, M., Bale, S. S., Bhushan, A., Hegde, M., ... Yarmush, M. L. (2014). A novel ultrathin collagen nanolayer assembly for 3-D microtissue engineering: Layer-by-layer collagen deposition for long-term stable microfluidic hepatocyte culture. *Technology*, 02(1), 67–74. <https://doi.org/10.1142/S2339547814500083>
- McCarty, W. J., Usta, O. B., & Yarmush, M. L. (2016). A microfabricated platform for generating physiologically-relevant hepatocyte zonation. *Scientific Reports*, 6, 26868. <https://doi.org/10.1038/srep26868>
- McKeown, S. R. (2014). Defining normoxia, physoxia, and hypoxia in tumours-implications for treatment response. *The British Journal of Radiology*, 87(1035), 20130676. <https://doi.org/10.1259/bjr.20130676>
- De Miguel, D., Gallego-Lleyda, A., Ayuso, J. M., Erviti-Ardanaz, S., Pazo-Cid, R., del Agua, C., ... Martinez-Lostao, L. (2016). TRAIL-coated lipid-nanoparticles overcome resistance to soluble recombinant TRAIL in nonsmall cell lung cancer cells. *Nanotechnology*, 27(18), 185101. <https://doi.org/10.1088/0957-4484/27/18/185101>
- Moreno-Manzano, V., Rodriguez-Jimenez, F. J., Acena-Bonilla, J. L., Fustero-Lardies, S., Erceg, S., Dopazo, J., ... Sanchez-Puelles, J. M. (2010). FM19G11, a new hypoxia-inducible factor (HIF) modulator, affects stem cell differentiation status. *Journal of Biological Chemistry*, 285(2), 1333–1342. <https://doi.org/10.1074/jbc.M109.008326>
- Nath, B., & Szabo, G. (2012). Hypoxia and hypoxia inducible factors: Diverse roles in liver diseases. *Hepatology*, 55(2), 622–633. <https://doi.org/10.1002/hep.25497>
- Paik, J. Y., Jung, K. H., Lee, J. H., Park, J. W., & Lee, K. H. (2017). Reactive oxygen species-driven HIF1 α triggers accelerated glycolysis in endothelial cells exposed to low oxygen tension. *Nuclear Medicine and Biology*, 45, 8–14. <https://doi.org/10.1016/j.nucmedbio.2016.10.006>
- Park, J., Berthiaume, F., Toner, M., Yarmush, M. L., & Tilles, A. W. (2005). Microfabricated grooved substrates as platforms for bioartificial liver reactors. *Biotechnology and Bioengineering*, 90(5), 632–644. <https://doi.org/10.1002/bit.20463>
- Polinkovsky, M., Gutierrez, E., Levchenko, A., & Groisman, A. (2009). Fine temporal control of the medium gas content and acidity and on-chip generation of series of oxygen concentrations for cell cultures. *Lab on a Chip*, 9(8), 1073–1084. <https://doi.org/10.1039/b816191g>
- Popovici, R. M., Lu, M., Bhatia, S., Faessen, G. H., Giaccia, A. J., & Giudice, L. C. (2001). Hypoxia regulates insulin-like growth factor-binding protein 1 in human fetal hepatocytes in primary culture-suggestive molecular mechanisms for in utero fetal growth restriction caused by uteroplacental insufficiency. *The Journal of Clinical Endocrinology & Metabolism*, 86(6), 2653–2659.
- Prodanov, L., Jindal, R., Bale, S. S., Hegde, M., McCarty, W. J., Golberg, I., ... Usta, O. B. (2016). Long-term maintenance of a microfluidic 3D human liver sinusoid. *Biotechnology and Bioengineering*, 113(1), 241–246. <https://doi.org/10.1002/bit.25700>
- Qin, H. H., Filippi, C., Sun, S., Lehec, S., Dhawan, A., & Hughes, R. D. (2015). Hypoxic preconditioning potentiates the trophic effects of mesenchymal stem cells on co-cultured human primary hepatocytes. *Stem Cell Research & Therapy*, 6, 237. <https://doi.org/10.1186/s13287-015-0218-7>
- Reichner, J. S., & Albina, J. E. (2004). Determination of the role of hypoxia-inducible factor 1 in wound healing. *Methods in Enzymology*, 381, 527–538. [https://doi.org/10.1016/S0076-6879\(04\)81034-6](https://doi.org/10.1016/S0076-6879(04)81034-6)
- Robinson, M. W., Harmon, C., & O'Farrelly, C. (2016). Liver immunology and its role in inflammation and homeostasis. *Cellular & Molecular Immunology*, 13(3), 267–276. <https://doi.org/10.1038/cmi.2016.3>
- Samanta, D., Gilkes, D. M., Chaturvedi, P., Xiang, L., & Semenza, G. L. (2014). Hypoxia-inducible factors are required for chemotherapy resistance of breast cancer stem cells. *Proceedings of the National Academy of Sciences of the United States of America*, 111(50), E5429–E5438. <https://doi.org/10.1073/pnas.1421438111>
- Sato, A., Kadokura, K., Uchida, H., & Tsukada, K. (2014). An in vitro hepatic zonation model with a continuous oxygen gradient in a microdevice. *Biochemical and Biophysical Research Communications*, 453(4), 767–771. <https://doi.org/10.1016/j.bbrc.2014.10.017>
- Schleicher, J., Dahmen, U., Guthke, R., & Schuster, S. (2017). Zonation of hepatic fat accumulation: Insights from mathematical modelling of nutrient gradients and fatty acid uptake. *Journal of the Royal Society, Interface*, 14(133), 20170443. <https://doi.org/10.1098/rsif.2017.0443>
- Seglen, P. O. (1976). Preparation of isolated rat liver cells. *Methods in Cell Biology*, 13(1), 29–83.
- Semenza, G. L. (2012). Hypoxia-inducible factors: Mediators of cancer progression and targets for cancer therapy. *Trends In Pharmacological Sciences*, 33(4), 207–214. <https://doi.org/10.1016/j.tips.2012.01.005>
- Sen, C. K. (2009). Wound healing essentials: Let there be oxygen. *Wound Repair and Regeneration*, 17(1), 1–18. <https://doi.org/10.1111/j.1524-475X.2008.00436.x>
- Shimizu, S., Eguchi, Y., Kamiike, W., Waguri, S., Uchiyama, Y., Matsuda, H., & Tsujimoto, Y. (1996). Retardation of chemical hypoxia-induced necrotic cell death by Bcl-2 and ICE inhibitors: Possible involvement of common mediators in apoptotic and necrotic signal transductions. *Oncogene*, 12(10), 2045–2050.
- Wolfe, D., Schmidt, H., & Jungermann, K. (1983). Short-term modulation of glycogen metabolism, glycolysis and gluconeogenesis by physiological oxygen concentrations in hepatocyte cultures. *European Journal of Biochemistry*, 135(3), 405–412.
- Yu, F., Deng, R., Hao Tong, W., Huan, L., Chan Way, N., IslamBadhan, A., ... Yu, H. (2017). A perfusion incubator liver chip for 3D cell culture with application on chronic hepatotoxicity testing. *Scientific Reports*, 7(1), 14528. <https://doi.org/10.1038/s41598-017-13848-5>
- Zhongbao, S., & Jingqi, Z. (2002). Influence of catalysts on deoxidation of Na₂SO₃. *Corrosion Science and Protection Technology*, 14(1), 3.